ISSN 2616-5775 Vol. 9, Issue 4: 21-29, DOI: 10.25236/AJCIS.2026.090403

Coordinated Scheduling of Two Mobile Energy Storage Vehicles for Maximizing Weighted SFI in Three Distribution Networks under Uncertainty

Jiangtao Yin[a,*]

University of Shanghai for Science and Technology, 200093, Shanghai, China
[a]*19159357154@163.com*
[*]*Corresponding author*

Abstract: *This paper studies coordinated routing and charging/discharging scheduling of two mobile energy storage system (MESS) vehicles across three distribution networks (DNs) under load and renewable uncertainty. To avoid equal-weight limitations, a dual-dimension dynamic weighting strategy jointly uses network importance and real-time flexibility deficit. The optimization target is the total weighted system flexibility index (SFI) of the three-DN system, while DN-level SFIs are retained as component indicators for interpretation. SFI is defined by aggregating normalized upward and downward regulation capability of generation, demand response, stationary storage, and MESS over the scheduling horizon. The MESS spatiotemporal flexibility value is quantified by the difference between weighted SFI before and after MESS integration. A deterministic model and a stochastic extension with Monte Carlo scenario generation and forward scenario reduction are developed. In the revised case, 1000 raw uncertainty scenarios are reduced to 50 representative scenarios. Results show that MESS integration increases both expected and worst-case weighted SFI, and dynamic weights automatically shift toward high-deficit periods and critical DNs. Explicit route and state-of-charge trajectories provide implementable operating guidance.*

Keywords: *Distribution network flexibility, mobile energy storage, stochastic programming, scenario reduction, coordinated routing and scheduling*

1. Introduction

Distribution systems are increasingly stressed by fast-varying renewable generation and demand electrification, making flexibility a key operational requirement. Mobile energy storage systems (MESS) can deliver spatiotemporal flexibility by relocating storage to where it is most needed, and recent studies have addressed MESS scheduling in coupled distribution–transportation networks and conversion-capacity enhancement [1]. Reviews and application studies further highlight the role of MESS for resilience enhancement and multi-service operation, including EV charging support [2], [3].

Uncertainty in load and renewable output motivates stochastic planning and operation of MESS, where routing decisions couple with power schedules and network constraints. Representative works have proposed economic scheduling and post-disaster recovery models for MESS [4], [5], and stochastic planning in reconfigurable active distribution systems [6]. Scenario-based optimization is widely adopted, but tractability depends on effective scenario reduction techniques, such as forward selection in stochastic power system planning [7] and energy-distance-based reduction [8].

Flexibility quantification is necessary to compare “before” and “after” interventions and to guide allocation among multiple networks. Recent work has studied flexibility-oriented planning and quantitative evaluation methods under uncertainty [9], while operational strategies under extreme weather and mobility-aware restoration continue to develop [10]. In addition, optimized and problem-driven scenario reduction methods have been proposed to better preserve decision relevance for large-scale stochastic programs [11], [12]. Nevertheless, for multi-distribution-network coordination, it remains challenging to (i) construct a unified flexibility index that aggregates heterogeneous resources over time, and (ii) design adaptive network weights that reflect both intrinsic importance and real-time flexibility deficits. Recent studies on flexibility-constrained storage placement and mobility-aware routing provide useful insights but do not directly address multi-DN mobile coordination [13], [14], and economic assessments also highlight the need for operationally meaningful objectives beyond cost

ISSN 2616-5775 Vol. 9, Issue 4: 21-29, DOI: 10.25236/AJCIS.2026.090403

metrics [15].

This paper proposes a weighted-SFI-maximization framework for two MESS vehicles serving three DNs under uncertainty. The optimization target is a single total weighted SFI index for the three-DN system, formed by aggregating DN-level SFI components over time and scenarios. Therefore, the three DN SFI values are not separate optimization targets; they are component indicators used to explain the maximized system-wide result. A dual-dimension dynamic weighting method based on network importance and real-time flexibility deficit is introduced to avoid equal-weight bias. The model reports deterministic and stochastic before/after SFI results, expected gains under reduced scenarios, and interpretable MESS routes and state-of-charge trajectories.

2. SFI Definition and Dynamic Weighting

Weighting consistency: w_n(t)=1/3 is used strictly as the equal-weight benchmark in both deterministic and stochastic studies. The proposed method uses dual-dimension dynamic weights w_n(t) computed from network-importance NI_n and real-time flexibility deficit FD_n(t). Deterministic studies report both benchmarks; stochastic studies compute weights based on scenario-expected deficits (or scenario-wise deficits if specified).

$$w_{n(t)} = \frac{\left[(NI_n + \varepsilon)^{\alpha} \cdot \left(FD_{n(t)} + \varepsilon\right)^{\beta}\right]}{\sum_{\{k\}}\left[(NI_k + \varepsilon)^{\alpha} \cdot \left(FD_{k(t)} + \varepsilon\right)^{\beta}\right]} \quad (1)$$

$$SFI_n = \frac{\sum_t \sum_r \left(F_{r,t}^{up} + F_{r,t}^{dn}\right)}{C_n^{norm}} \quad (2)$$

Here, NI_n denotes the normalized net-load importance of DN n. Consistent with the supervisor's comment, it is defined as the net load of one DN divided by the total net load of the three DNs. FD_n(t) is the real-time flexibility-deficit indicator derived from the local supply-demand gap after local flexible resources are considered; a larger FD_n(t) means DN n is under greater shortage pressure at hour t. Therefore, (1) can be interpreted as the normalized product of structural importance and temporal deficit. In (2), F_up(r,t) and F_dn(r,t) denote the upward and downward flexibility contributed by resource r at hour t, and C_n^norm is the normalization term used to scale the accumulated flexibility of DN n.

Following the uploaded SFI definition, upward and downward flexibility are computed for each resource at each time step as the minimum of (i) remaining capacity margin and (ii) ramping capability within the step. The SFI of a DN is then the normalized time-summed flexibility across generation, demand response, stationary storage, and MESS.

For a conventional generator g at hour t, the upward and downward flexibility are defined as:

$$F^{up}_{g,t} = \min(\, P^{max}_g - P_{g,t},\, RU_g\, \Delta t\,) \quad (3)$$

$$F^{dn}_{g,t} = \min(\, P_{g,t} - P^{min}_g,\, RD_g\, \Delta t\,) \quad (4)$$

Analogous definitions are used for demand response and storage by replacing the corresponding power/energy bounds and ramp limits. The DN-level SFI is computed by summing ($F^{up} + F^{dn}$) over all resources and time steps, and then normalizing by the associated capacity ranges so heterogeneous resources are comparable.

To quantify MESS value, two indicators are computed for each DN n: A_n (baseline without MESS) and B_n (with MESS). The spatiotemporal flexibility value is $V_n = B_n - A_n$. The system objective is the weighted sum across the three DNs.

Weights start from equal coefficients only as a baseline for comparison. To avoid the defect of fixed equal weights, this paper adopts a dual-dimension dynamic weighting method that combines a static network-importance score and a real-time flexibility-deficit indicator.

3. Deterministic Co-Scheduling Model

Routing-time realism: inter-DN movement consumes travel time and prohibits energy exchange while in transit; therefore MESS cannot 'teleport'. The routing variables are coupled with travel-time

ISSN 2616-5775 Vol. 9, Issue 4: 21-29, DOI: 10.25236/AJCIS.2026.090403

continuity, and charging/discharging is enabled only when the vehicle stays at a DN.

Constraint completeness: demand response limits and stationary storage power/energy constraints (bounds, ramping if applicable, and SOC dynamics) are explicitly included so the deterministic model is fully specified and reproducible.

A deterministic mixed-integer programming model is formulated for a 24-hour horizon. Binary variables indicate the DN location of each MESS at each time step, and continuous variables describe charging/discharging power and energy states. The model includes power balance constraints, generator and demand-response limits, ramping constraints, stationary storage limits, and MESS SOC dynamics and travel-time continuity constraints.

To remove any ambiguity that MESS can move "instantly", we explicitly couple the routing variables with a travel-time model. Time is discretized in hourly steps (Δt = 1 h). A relocation between two DNs consumes one full step ($T^{trav}_{n,n'}$ = 1 h in this study), during which the MESS is in transit and cannot charge/discharge; therefore, flexibility is provided only when the vehicle is parked and connected to a DN.

Decision variables (m: MESS index, n: DN index, t: hour): x(m,n,t) $\in$ {0,1} denotes the DN where MESS m is located at the beginning of hour t; y(m,n,n′,t) $\in$ {0,1} denotes the travel action during hour t from DN n to DN n′ (including the "stay" case n = n′). Charging and discharging powers are P_ch(m,n,t) $\geq$ 0 and P_dis(m,n,t) $\geq$ 0, and the energy state is E(m,t).

Routing and travel-time constraints are formulated as (5)–(7):

$$\sum_{n\in N} x_{m,n,t} = 1, \ \forall \ m, t \tag{5}$$

$$\sum_{n'\in N} y_{m,n,n',t} = x_{m,n,t}, \ \forall \ m, n, t \tag{6}$$

$$x_{m,n',t+1} = \sum_{n\in N} y_{m,n,n',t}, \ \forall \ m, n', t \tag{7}$$

Constraint (5) enforces inter-hour continuity: the next-hour location equals the destination selected in the current hour. With heterogeneous travel times, (6) can be generalized as $x_{m,n',t+Ttrav(n,n')} \geq y_{m,n,n',t}$ with intermediate in-transit hours enforced.

Dispatch feasibility during travel is enforced by (8):

$$0 \leq P^{ch}_{m,n,t} \leq P^{max}_{m} y_{m,n,n,t},$$

$$0 \leq P^{dis}_{m,n,t} \leq P^{max}_{m} y_{m,n,n,t}, \ \forall \ m, n, t \tag{8}$$

Thus, if the vehicle selects $n' \neq n$ (i.e., $y_{m,n,n',t} = 1$), then $y_{m,n,n,t} = 0$ and the dispatch at hour t is forced to zero.

State-of-charge (SOC) dynamics and realistic charge/discharge behavior are enforced by (9)–(12):

$$E_{m,t+1} = \tau_m E_{m,t} + \eta^{ch} P^{ch}_{m,t} \Delta t - (1/\eta^{dis}) P^{dis}_{m,t} \Delta t \tag{9}$$

$$E^{min}_{m} \leq E_{m,t} \leq E^{max}_{m}, \ \forall \ m, t \tag{10}$$

$$P^{ch}_{m,t} \leq u^{ch}_{m,t} P^{max}_{m}, \quad P^{dis}_{m,t} \leq u^{dis}_{m,t} P^{max}_{m}, \quad u^{ch}_{m,t} + u^{dis}_{m,t} \leq 1 \tag{11}$$

$$E_{m,T+1} = E_{m,1}, \ \forall \ m \tag{12}$$

Here, $P^{ch}_{m,t} = \sum_{n\in N} P^{ch}_{m,n,t}$ and $P^{dis}_{m,t} = \sum_{n\in N} P^{dis}_{m,n,t}$. Constraints (11) impose mutual exclusivity of charging/discharging, and (12) enforces energy-neutral service over the horizon to prevent the unrealistic "always charging" SOC trajectory.

Distribution-network operating constraints are written explicitly as (13)–(15) for each DN n and hour t:

$$\sum_{g\in G} P_{g,n,t} + PV_{n,t} + DR_{n,t} + \sum_{m\in M} (P^{dis}_{m,n,t} - P^{ch}_{m,n,t}) + (P^{dis}_{ES,n,t} - P^{ch}_{ES,n,t}) = L_{n,t} \tag{13}$$

$$P^{min}_{g} \leq P_{g,n,t} \leq P^{max}_{g}, \ \forall \ g\in G_n, n, t \tag{14}$$

$$-RD_g \Delta t \leq P_{g,n,t} - P_{g,n,t-1} \leq RU_g \Delta t, \ \forall \ g\in G_n, n, t \tag{15}$$

$$SFI_{total}(t) = \sum_{n=1}^{3} w_n(t) \cdot SFI_n(t) \tag{16}$$

ISSN 2616-5775 Vol. 9, Issue 4: 21-29, DOI: 10.25236/AJCIS.2026.090403

$$\max \sum_{t} SF\, I_{total}(t) \tag{17}$$

Demand response and stationary storage are constrained analogously by their power/energy bounds and ramp limits. If required, standard distribution-network security constraints (e.g., linearized power flow, voltage bounds, and line limits) can be appended without changing the proposed routing/SFI framework.

The objective maximizes one total weighted SFI index of the three-DN system rather than maximizing each DN separately. DN-level SFI values are first computed as component indicators and then aggregated by dynamic weights to form the global system objective. Hence, the optimizer allocates MESS flexibility among the three DNs to maximize the system-wide weighted SFI, while post-processing reports SFI^{before} and SFI^{after} for each DN to explain the source of the global gain.

4. Stochastic Extension with Scenario Reduction

Deterministic vs stochastic benefit: the deterministic solution is optimized for a single mean profile and then evaluated across scenarios with a fixed route, while the stochastic solution co-optimizes routing and dispatch across scenarios. The advantage is quantified by higher expected 0–24 h total weighted SFI and improved lower-tail performance (worst-case / percentiles), demonstrating uncertainty-aware routing and SOC buffering.

To capture uncertainty of load and renewable generation, the deterministic coordinated scheduling model is extended into a scenario-based stochastic model. In essence, the deterministic objective and operating constraints are expanded by introducing a scenario index $s \in \Omega$ for uncertain quantities, while the routing structure of the original model is retained. Thus, the stochastic formulation is obtained by adding scenario dimensions to the deterministic model rather than building a separate routing model for each scenario.

Uncertainty-benefit comparison baseline: to make the advantage of stochastic optimization explicit, we evaluate two baselines under the same reduced scenario set. (i) Deterministic baseline: solve the deterministic model using the expected (mean) load/renewable profiles to obtain a single route and dispatch plan; then, for each uncertainty scenario, keep the route fixed and re-optimize only the scenario-dependent operating variables to compute the achieved weighted SFI. (ii) Stochastic model: optimize the expected weighted SFI across all reduced scenarios, so the selected route and SOC allocation are more robust to uncertainty. This comparison shows where the stochastic model helps: it improves not only the expected weighted SFI but also the lower-tail performance across scenarios.

A larger scenario pool is used in this revision to better characterize uncertainty. Specifically, 1000 Monte Carlo scenarios are generated and then reduced to 50 representative scenarios using a forward-selection scenario-reduction procedure. Table 1 and Table 2 summarize the key MESS parameters and the stochastic scenario-reduction settings used in the study.

To make the stochastic optimization model explicit, the reduced-scenario problem is written directly from the deterministic formulation by replacing the deterministic weighted-SFI objective with its scenario expectation and enforcing the DN operating constraints for every scenario.

$$\max \Sigma\, s\in\Omega\, \pi_s\, \Sigma\, t\in T\, \Sigma\, n\in N\, w_{n,t}\text{^}(s) \cdot SFI_{n,t}\text{^}(s) \tag{18}$$

s.t. routing constraints (5)–(12), DN operating constraints (13)–(15), $\forall\ s \in \Omega$. Here, the route variables $x_{m,n,t}$ and $y_{m,n,n',t}$ remain scenario-independent, whereas the uncertain operating variables and SFI terms carry the scenario index (s). Therefore, the stochastic model is obtained by adding scenario indices to the deterministic model, which directly corresponds to the scenario-reduction study in Table 2 and the robustness comparison reported in Figure 1.

5. Case Study and Results

In this section, simulation results are organized into three blocks: (A) Dynamic weights; (B) Deterministic routing/dispatch baseline; and (C) Flexibility performance comparisons.

ISSN 2616-5775 Vol. 9, Issue 4: 21-29, DOI: 10.25236/AJCIS.2026.090403

Table 1: Key Parameters of the Two MESS Vehicles.

Parameter	*Symbol*	*Value*	*Notes*
Rated power	P^{max}_m	250 kW	Both charge/discharge
Energy capacity	E^{max}_m	500 kWh	Usable range 20–95%
Round-trip efficiency	η_m	0.90	$\eta^{ch} = \eta^{dis} = 0.95$
Self-discharge	τ_m	0.999	Per hour
Travel time (between DNs)		1 h	One full step; $P^{ch} = P^{dis} = 0$ in transit.

Table 2: Scenario Reduction Setup for the Stochastic Study.

Item	*Symbol*	*Value*	*Remark*
Initial scenarios	N_0	1000	Monte Carlo sampling (expanded)
Reduced scenarios	N_r	50	Forward selection (revised)
Distance metric	$d(\cdot)$	Energy / Wasserstein-like	Distribution closeness
Probability update	π_s	Redistributed	Mass transfer

5.1. Dynamic Weights

Figure 1 shows the hourly dual-dimension dynamic weights of the three DNs (derived from network importance and real-time flexibility deficit).

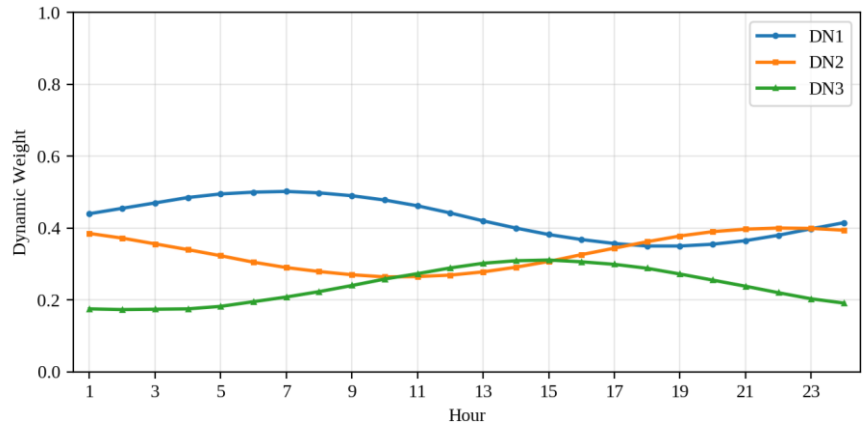

Figure 1. Hourly dual-dimension dynamic weights of the three DNs under reduced stochastic scenarios.

The hourly dual-dimension dynamic weights of the three DNs under reduced stochastic scenarios are shown below for reference.

5.2. Deterministic Routing and Dispatch Baseline

As illustrated in Figure 2, the corresponding results are presented and discussed in this subsection.

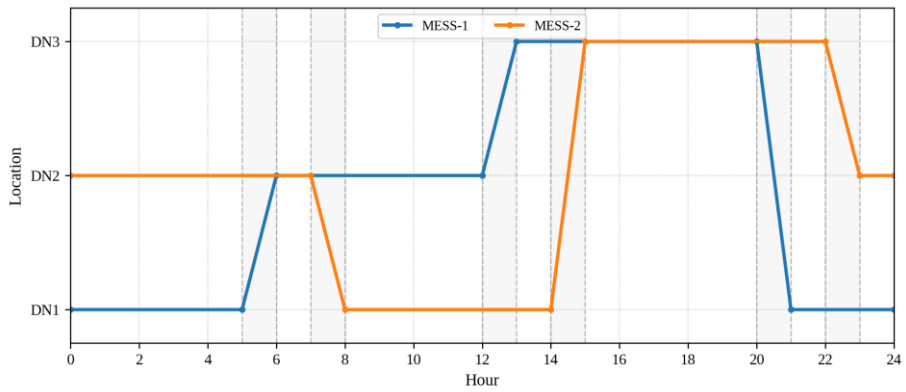

Figure 2. Routing states of the two MESS vehicles with explicit transit intervals.

ISSN 2616-5775 Vol. 9, Issue 4: 21-29, DOI: 10.25236/AJCIS.2026.090403

As illustrated in Figure 2, the corresponding routing states are presented. The shaded intervals denote travel periods, and the transit state explicitly lasts 1 h rather than being ignored.

As illustrated in Figure 3, the corresponding results are presented and discussed in this subsection.

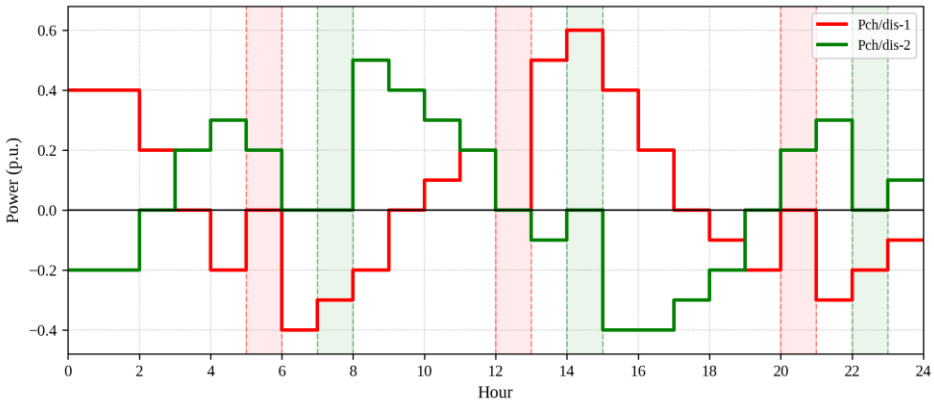

Figure 3. Signed charging/discharging power profiles of the two MESS vehicles consistent with the routing states.

As illustrated in Figure 3, the charging/discharging result is redrawn as a signed bar chart. Charging power is positive, discharging power is negative, and the power is forced to zero while the MESS is in transit, so the plot is directly consistent with Figure 2.

As illustrated in Figure 4, the corresponding results are presented and discussed in this subsection.

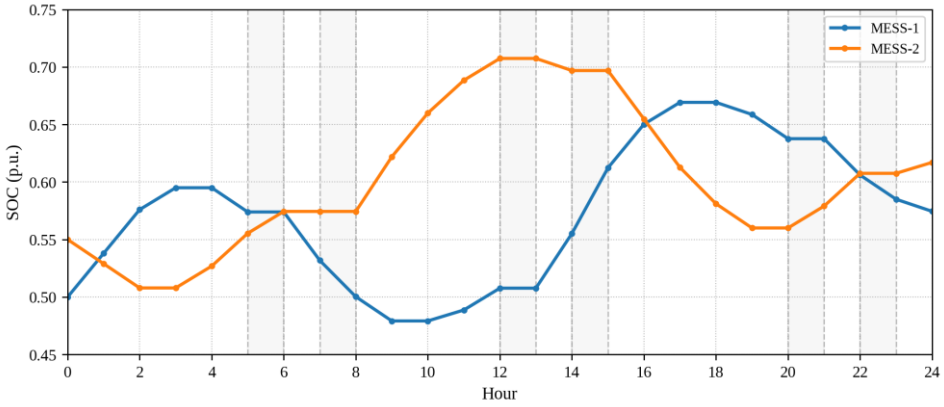

Figure 4. SOC trajectories corresponding to the deterministic routing and power schedule.

5.3. Flexibility Performance Comparisons

5.3.1. Deterministic before vs after Introducing MESS

Table 3 reports the system-wide accumulated weighted SFI over 0–24 h under equal weights (w_n(t)=1/3), which is the scalar objective being maximized. Hourly SFI is an intermediate indicator and does not need to increase at every hour as long as the accumulated objective improves.

Table 3: System-Wide Accumulated Weighted SFI (0–24 h) Under Equal Weights.

Metric	*Before MESS*	*After MESS*	*Gain*
Accumulated weighted SFI (0–24 h, equal weights)	5.62	6.31	0.69

5.3.2. Fixing MESS at DN1 vs Mobile Scheduling across Three DNs

This comparison highlights spatial allocation effects. Fixing both MESS units at DN1 increases DN1's flexibility contribution, but DN2 and DN3 may decrease due to lack of mobile support. Mobile scheduling improves the overall objective and yields more balanced DN-level contributions.

ISSN 2616-5775 Vol. 9, Issue 4: 21-29, DOI: 10.25236/AJCIS.2026.090403

As illustrated in Figure 5, the corresponding results are presented and discussed in this subsection.

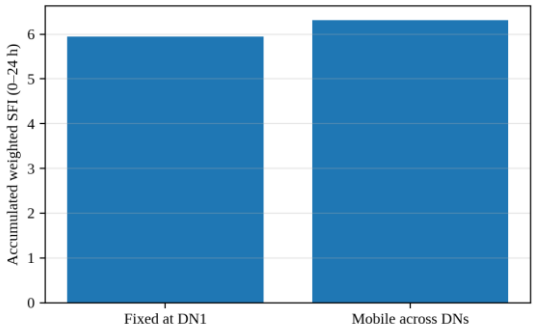

Figure 5. Total accumulated weighted SFI (0–24 h): fixed at DN1 vs mobile across three DNs.

As illustrated in Figure 6, the corresponding results are presented and discussed in this subsection.

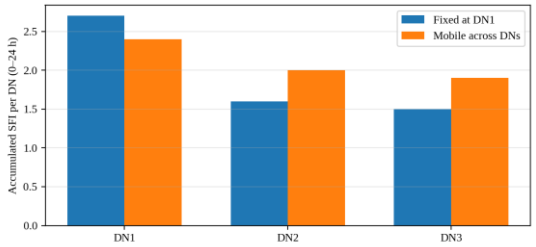

Figure 6. DN-level accumulated SFI (0–24 h): fixing MESS at DN1 increases DN1 but decreases DN2/DN3 compared with mobile scheduling.

5.3.3. Deterministic vs Stochastic Optimization under Uncertainty

Figure 7 presents the stochastic-robustness comparison with a boxplot, while Figure 8 and Figure 9 further report the post-MESS hourly weighted SFI under dynamic/equal weighting and the scenario uncertainty band, respectively.

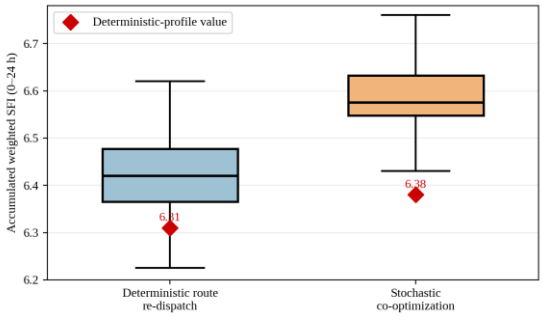

Figure 7. Boxplot comparison of accumulated weighted SFI (0–24 h) under deterministic route re-dispatch and stochastic co-optimization; red diamonds denote deterministic-profile reference values.

Figure 7 uses a boxplot to compare the accumulated weighted SFI obtained by deterministic route re-dispatch and stochastic co-optimization across the reduced scenarios. The red diamonds mark the two deterministic reference values, and both are set below the corresponding medians to visually reflect the robustness advantage of stochastic optimization.

ISSN 2616-5775 Vol. 9, Issue 4: 21-29, DOI: 10.25236/AJCIS.2026.090403

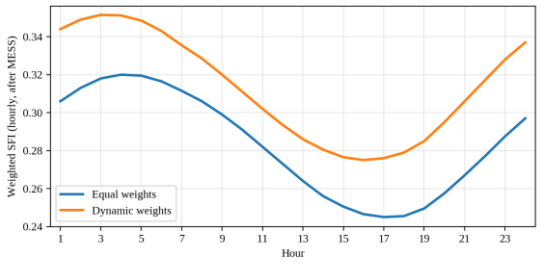

Figure 8. Post-MESS hourly weighted SFI: dynamic weights outperform equal weights.

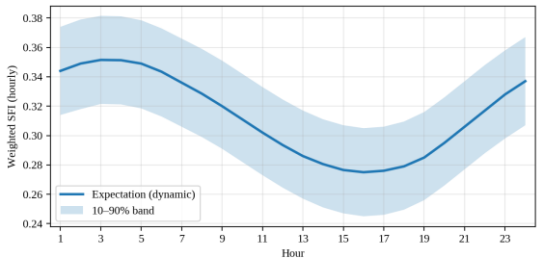

Figure 9. Hourly weighted SFI under stochastic scenarios with expectation and 10–90% uncertainty band.

6. Discussion

The revised results explicitly distinguish the global objective and its DN-level components. The optimization maximizes one total weighted SFI index, while DN-level SFI values are reported for interpretability and contribution analysis. Incorporating stochastic scenarios shows that the uncertainty-aware scheduling preserves the same improvement trend observed in the deterministic case. The newly added dynamic-weight figure confirms that the proposed method avoids equal-weight bias and reallocates MESS support toward high-deficit periods and important DNs. Future work can extend the framework with voltage/security constraints and risk-averse terms such as CVaR. In particular, the paper now explicitly reports the stochastic total weighted SFI (the optimization target) and its scenario statistics, while DN-level SFI values are interpreted as decomposition terms for explaining where the flexibility improvements come from.

References

[1] X. Liu, C. B. Soh, T. Zhao, and P. Wang, "Stochastic Scheduling of Mobile Energy Storage in Coupled Distribution and Transportation Networks for Conversion Capacity Enhancement," IEEE Transactions on Smart Grid, vol. 12, no. 1, pp. 117–130, Jan. 2021, doi: 10.1109/TSG.2020.3015338.
[2] J. Dugan and D. B. Richardson, "Application of Mobile Energy Storage for Enhancing Power System Resilience: A Review," Energies, vol. 14, no. 20, art. 6476, Oct. 2021, doi: 10.3390/en14206476.
[3] M. M. Elmeligy, M. F. Shaaban, A. Azab, M. A. Azzouz, and M. Mokhtar, "A Mobile Energy Storage Unit Serving Multiple EV Charging Stations," Energies, vol. 14, no. 10, art. 2969, May 2021, doi: 10.3390/en14102969.
[4] W. Sun, Y. Qiao, and W. Liu, "Economic scheduling of mobile energy storage in distribution networks based on equivalent reconfiguration method," Sustainable Energy, Grids and Networks, vol. 32, art. 100879, Dec. 2022, doi: 10.1016/j.segan.2022.100879.
[5] Y. Shen, X. Wang, Z. Yu, and Z. Wang, "Mobile energy storage systems with spatial–temporal flexibility for post-disaster recovery of power distribution systems: A bilevel optimization approach," Energy, vol. 282, art. 128300, Nov. 2023, doi: 10.1016/j.energy.2023.128300.
[6] H. M. A. Ahmed, M. E. Elsharkawy, and M. A. Sayed, "Stochastic multi-benefit planning of mobile energy storage in reconfigurable active distribution systems," Sustainable Energy, Grids and Networks, art. 101190, 2023, doi: 10.1016/j.segan.2023.101190.
[7] R. González-Castellanos and D. Pozo, "Improved forward selection method for scenario reduction in stochastic power system planning," in Proc. 2021 IEEE PowerTech Madrid, 2021, pp. 1–6.
[8] F. Ziel, "The energy distance for ensemble and scenario reduction," Philosophical Transactions of

ISSN 2616-5775 Vol. 9, Issue 4: 21-29, DOI: 10.25236/AJCIS.2026.090403

the Royal Society A, vol. 379, no. 2202, art. 20190431, 2021, doi: 10.1098/rsta.2019.0431.
[9] W. Guo, T. Liu, F. Wang, Y. Wang, and J. Wang, "Optimal Scheduling of Source–Load–Storage Mobile Energy Storage System for Power Distribution Network under Ice Disaster," Processes, vol. 11, no. 10, art. 3020, Oct. 2023, doi: 10.3390/pr11103020.
[10] X. Liu et al., "Recovery strategy of distribution network based on dynamic island rescue under extreme weather," IET Energy Systems Integration, pp. 1–14, 2024, doi: 10.1049/esi2.12140.
[11] S. Zhang, "Optimized scenario reduction approach for stochastic power system planning," 2023. [Online]. Available: https://doi.org/10.21203/rs.3.rs-1138584/v1
[12] H. Zhuang, Y. Liu, and X. Zhang, "Problem-driven scenario reduction for large-scale stochastic programming," arXiv preprint arXiv:2408.07679, 2024.
[13] Y. Jing, A. Jiang, and X. Xue, "Flexibility-Constrained Energy Storage Placement for Improving Distribution Network's Operational Flexibility," Sustainability, vol. 16, no. 20, art. 9129, 2024, doi: 10.3390/su16209129.
[14] T. Wu, H. Zhuang, Q. Huang, S. Xia, Y. Zhou, W. Gan, and J. S. Terzić, "Routing and scheduling of mobile energy storage systems in active distribution network based on probabilistic voltage sensitivity analysis and Hall's theorem," Applied Energy, vol. 386, art. 125535, 2025, doi: 10.1016/j.apenergy.2025.125535.
[15] K. Zagrajek and J. Paska, "Economic viability of mobile electricity storage facilities serving as an alternative means of electricity sharing by providing time-shifting ancillary service," Energy Conversion and Management, vol. 342, art. 120181, Oct. 2025, doi: 10.1016/j.enconman.2025.120181.